Analysis of Circulating Cell-Free DNA Identifies Multiclonal Heterogeneity of *BRCA2* Reversion Mutations Associated with Resistance to PARP Inhibitors

David Quigley[1,2], Joshi J. Alumkal[3,4], Alexander W. Wyatt[5], Vishal Kothari[1,6], Adam Foye[1,7], Paul Lloyd[1,7], Rahul Aggarwal[1,7], Won Kim[1,7], Eric Lu[3], Jacob Schwartzman[3], Kevin Beja[5], Matti Annala[5,8], Rajdeep Das[1,6], Morgan Diolaiti[1], Colin Pritchard[9], George Thomas[3,10], Scott Tomlins[11], Karen Knudsen[12], Christopher J. Lord[13], Charles Ryan[1,7], Jack Youngren[1,7], Tomasz M. Beer[3], Alan Ashworth[1,14], Eric J. Small[1,7], and Felix Y. Feng[1,6]

ABSTRACT

Approximately 20% of metastatic prostate cancers harbor mutations in genes required for DNA repair by homologous recombination repair (HRR) such as *BRCA2*. HRR defects confer synthetic lethality to PARP inhibitors (PARPi) such as olaparib and talazoparib. In ovarian or breast cancers, olaparib resistance has been associated with HRR restoration, including by *BRCA2* mutation reversion. Whether similar mechanisms operate in prostate cancer, and could be detected in liquid biopsies, is unclear. Here, we identify *BRCA2* reversion mutations associated with olaparib and talazoparib resistance in patients with prostate cancer. Analysis of circulating cell-free DNA (cfDNA) reveals reversion mutation heterogeneity not discernable from a single solid-tumor biopsy and potentially allows monitoring for the emergence of PARPi resistance.

SIGNIFICANCE: The mechanisms of clinical resistance to PARPi in DNA repair–deficient prostate cancer have not been described. Here, we show *BRCA2* reversion mutations in patients with prostate cancer with metastatic disease who developed resistance to talazoparib and olaparib. Furthermore, we show that PARPi resistance is highly multiclonal and that cfDNA allows monitoring for PARPi resistance. *Cancer Discov; 7(9); 999–1005. ©2017 AACR.*

See related commentary by Domchek, p. 937.
See related article by Kondrashova et al., p. 984.
See related article by Goodall et al., p. 1006.

[1]Helen Diller Family Comprehensive Cancer Center, University of California, San Francisco (UCSF), San Francisco, California. [2]Department of Epidemiology and Biostatistics, UCSF, San Francisco, California. [3]Knight Cancer Institute, Oregon Health & Science University, Portland, Oregon. [4]Department of Molecular and Medical Genetics, Oregon Health & Science University, Portland, Oregon. [5]Vancouver Prostate Centre, Department of Urologic Sciences, University of British Columbia, British Columbia, Canada. [6]Department of Radiation Oncology, UCSF, San Francisco, California. [7]Division of Hematology and Oncology, UCSF, San Francisco, California. [8]Institute of Biosciences and Medical Technology, University of Tampere, Tampere, Finland. [9]Department of Laboratory Medicine, University of Washington, Seattle, Washington. [10]Department of Pathology, Oregon Health & Science University, Portland, Oregon. [11]Department of Pathology, University of Michigan School of Medicine, Ann Arbor, Michigan. [12]Department of Cancer Biology, Sidney Kimmel Cancer Center, Thomas Jefferson University, Philadelphia, Pennsylvania. [13]The CRUK Gene Function Laboratory and Breast Cancer Now Research Centre, The Institute of Cancer Research, London, United Kingdom. [14]Department of Medicine, UCSF, San Francisco, California.

Note: Supplementary data for this article are available at Cancer Discovery Online (http://cancerdiscovery.aacrjournals.org/).

D. Quigley and J.J. Alumkal contributed equally to this article.

Corresponding Authors: Felix Y. Feng, UCSF Helen Diller Family Comprehensive Cancer Center, Box 0128, San Francisco, CA 94158. Phone 415-502-7222; E-mail: Felix.Feng@ucsf.edu; Eric J. Small, Eric.Small@ucsf.edu; and Alan Ashworth, Alan.Ashworth@ucsf.edu

doi: 10.1158/2159-8290.CD-17-0146

INTRODUCTION

Men who carry heterozygous deleterious germline mutations in *BRCA2* are predisposed to aggressive prostate cancer (1–4). Metastatic prostate tumors that arise in these patients frequently lose their remaining functional *BRCA2* allele (4, 5). Lack of functional wild-type BRCA2 is associated with defects in the repair of double-strand DNA breaks using homologous recombination repair (HRR) and with a characteristic mutational spectrum (6, 7). Cells lacking HRR must repair double-strand DNA breaks through more error-prone forms of DNA repair such as nonhomologous end joining. HRR-deficient tumors show increased sensitivity to drugs such as platinum salts and inhibitors of the DNA repair protein PARP1 (PARPi) that induce double-strand breaks by stalling replication forks and causing replication fork collapse (8, 9).

PARPi agents, including olaparib and talazoparib, inhibit PARP enzymatic function and trap PARP1 protein on damaged DNA (10). Multiple mechanisms of resistance to PARPi have been proposed (reviewed in ref. 11). Among these, secondary reversion mutations in the *BRCA1/2* genes have been associated with clinical resistance to platinum or olaparib (12–14). However, the mechanism of resistance in prostate cancer, and to PARPi other than olaparib, is unknown.

RESULTS

We studied a patient (patient 1) who harbored a germline *BRCA2* mutation (p.K1872X, chr13:32,914,106 A→T). This mutation introduces a premature stop codon in *BRCA2* exon 11 by converting a lysine codon (AAA) to a stop codon (TAA), truncating the encoded protein at residue p.1872. Patient 1 was initially diagnosed with a Gleason 6 localized prostate cancer and was treated with radiotherapy in 2009. His disease subsequently recurred and progressed despite a series of androgen-directed therapies, including nilutamide, enzalutamide, and abiraterone. In June 2014, he underwent biopsy of a bone metastasis as part of a research protocol and was then treated with the PARPi talazoparib, to which his disease initially responded. The prostate-specific antigen (PSA) of patient 1 decreased from 16.52 at talazoparib initiation to a nadir of 0.66 after 3 months on treatment (Fig. 1A). However, after seven and a half months of treatment, radiographic and PSA testing showed disease progression. A second metastatic biopsy, this time from the liver, was obtained at this time.

First, we performed mutation and DNA copy-number analysis on DNA extracted from the pre-talazoparib and resistant solid-tumor biopsies. Tumor content was estimated at greater than 60% by histopathologic review of tumor sections (Fig. 1B) and variant allele frequency analysis. We identified extensive genome-wide LOH and the presence of the BRCA-associated mutation signature three (6), both signature hallmarks of HRR deficiency (ref. 15; Supplementary Figs. S1–S3). The pathogenic p.K1872X *BRCA2* allele frequency in this sample was 65%, compared with 50% in the germline DNA sample, and only a single copy of the *BRCA2* locus was present in pre-talazoparib DNA, suggesting loss of the wild-type allele (Supplementary Fig. S2, Fig. 1C). Loss of wild-type *BRCA2* would be expected to sensitize the tumor to talazoparib, consistent with the observed decrease in PSA after treatment initiation (Fig. 1A). The resistant biopsy bore two secondary mutant *BRCA2* alleles that carried deletions of 177 and 66 nucleotides, respectively. Each allele eliminated the pathogenic p.K1872X mutation and removed 59 or 22 amino acids from the predicted encoded protein, while restoring the open reading frame to encode the critical C terminal region of *BRCA2* (Fig. 1C, labeled *D1* and *D2*, Supplementary Tables S1 and S2). Alleles *D1* and *D2* were predicted to produce proteins 3,359 and 3,396 amino acids in length that carried an altered BRC repeat domain 7 (Fig. 1D). Previous observations suggest that these altered proteins would highly likely restore HRR function and be resistant to talazoparib (12). Reversion deletions in *BRCA2* that eliminate BRC repeats 5 to 8 have been shown in cell line models to produce BRCA2 proteins with sufficient HRR function to confer cisplatin and PARPi resistance (12, 13). We confirmed that alleles *D1* and *D2* were exclusively present in the resistant tumor biopsy and not the pre-talazoparib or germline DNA by PCR amplification (Fig. 1E). These observations suggest that these alleles were not present in these samples until after talazoparib therapy was initiated.

Targeted sequencing of circulating cell-free DNA (cfDNA) was performed on plasma that was collected from patient 1 when the resistant liver biopsy was performed. At a local read depth of 200x, 48 DNA reads (24%) bore the p.K1872X allele, whereas 38 reads (19%) bore the wild-type allele. We identified 7 DNA fragments corresponding to deletion *D1*, 37 fragments corresponding to *D2*, and 5 additional deletion alleles not observed in the solid tumor (Fig. 1C, labeled *D3* through *D7*, Supplementary Tables S1 and S2). A total of 84 reads, when aligned to the genome, contained deletion alleles *D1* through *D7*, accounting for the valley in read depth visible at this locus (Fig. 1C). All deletion alleles eliminated the pathogenic p.K1872X mutation and restored the open reading frame of *BRCA2*, producing predicted proteins of residue length 3,409 to 3,212 compared with the 3,418 amino acid full-length BRCA2 protein. Notably, deletion *D4* was observed in cfDNA more than 4 times as frequently as deletion *D1*, but *D4* was observed zero times in the solid biopsy. Targeted sequencing of a paraffin section isolated from a physically distinct portion of the resistant liver biopsy using an orthogonal sequencing technology (Ion Torrent) at 1,000x coverage depth identified deletion *D1* but not deletion *D4* (Supplementary Tables S1 and S2). Applying this approach to a paraffin-embedded biopsy of patient 1's metastatic lesion that was obtained before talazoparib therapy did not identify any of the deletions in Fig. 1C. These observations raised the possibility that deletions other than *D1* and *D2* originated from a distinct metastasis that was not biopsied, or from a physically separate region of the same metastasis.

We next analyzed cfDNA isolated from a second prostate cancer case. Patient 2 was diagnosed with widespread metastatic prostate cancer in 2013 and progressed on numerous systemic therapies, including leuprolide, bicalutamide, enzalutamide, abiraterone, and eventually docetaxel. In late 2015, germline genetic testing demonstrated that he carried a germline heterozygous deletion of two nucleotides in *BRCA2* (p.R259fs) that introduced a stop-gain prematurely truncating the protein at residue 274. The PSA of patient 2 decreased on olaparib treatment from 355 to 42 after 4 months of

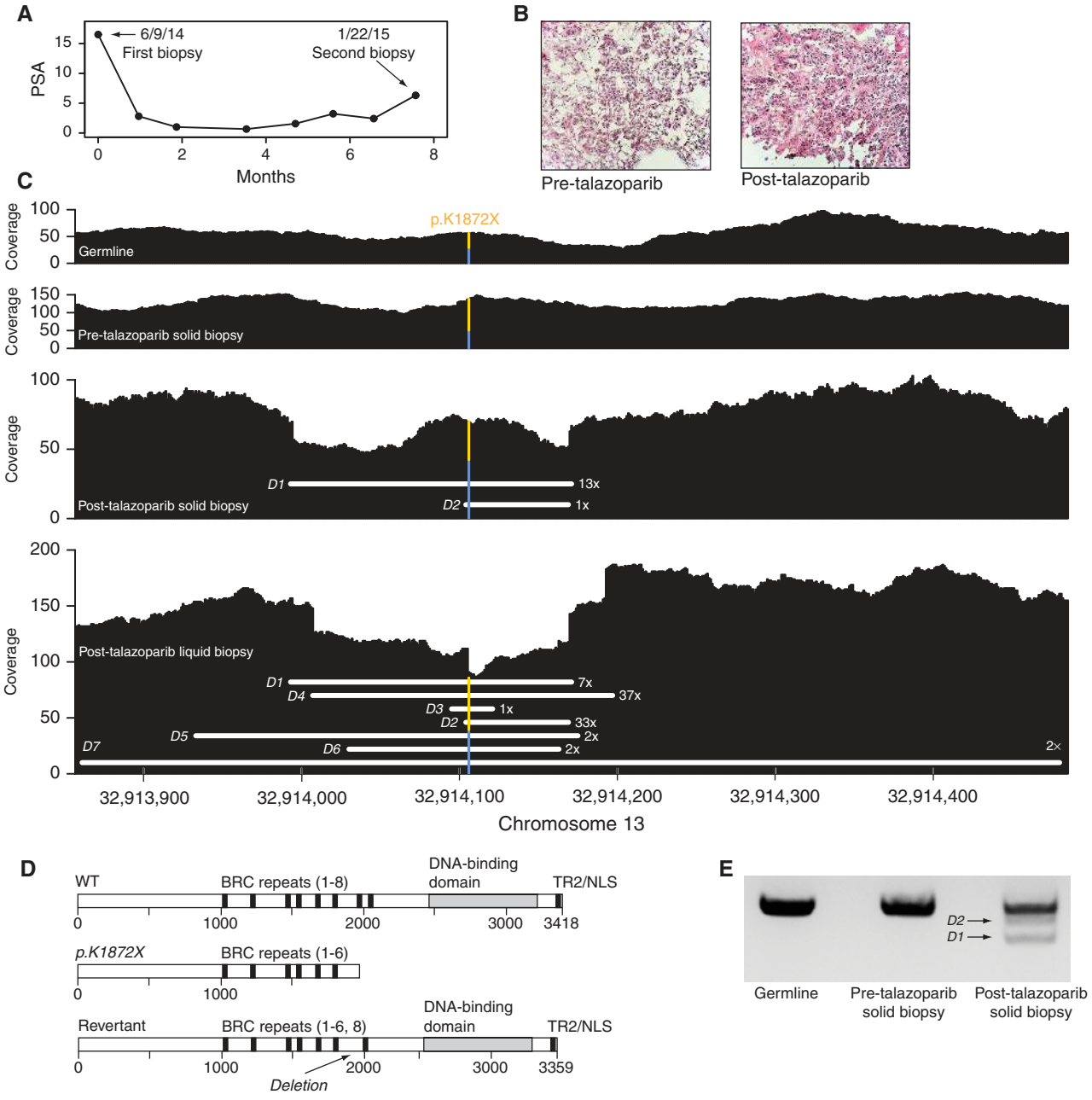

Figure 1. PARPi resistance by multiple large deletions. **A,** Timeline of patient 1's serum PSA level before and during treatment with talazoparib. **B,** Hematoxylin and eosin stains of the solid-tumor biopsy pre- and post-talazoparib were consistent with approximately 60% tumor purity. **C,** DNA read coverage of patient 1's germline, pre- and post-talazoparib solid-tumor, and post-talazoparib liquid biopsy. Horizontal white lines indicate the span of deletions, numbered *D1* through *D7*, with deletion frequency indicated at the right side. The location and frequency of the p.K1872X/wild-type allele are noted in gold/blue. **D,** Schematic protein models for BRCA2 wild-type (WT), p.K1872X, and reversion isoforms. **E,** PCR amplification of the region around deletions *D1* and *D2* in patient 1's germline, pre-talazoparib, and post-talazoparib solid biopsy confirms the presence of deletions *D1* and *D2* in post-talazoparib DNA.

treatment, with a nadir of 40.63 (Fig. 2A). Scans at 4 months of treatment showed a radiographic response (decrease in size of bony lesions, visceral lesions, and lymphadenopathy) and functional improvement (Eastern Cooperative Oncology Group score improvement from 2 to 1; Fig. 2B and C). However, by 7 months of treatment, the patient's PSA had reached 96.10, and a repeat bone scan at that time demonstrated numerous new bone and hepatic metastases (Fig. 2C).

DNA copy-number analysis of cfDNA of patient 2 identified single copy loss at the *BRCA2* locus (Supplementary Fig. S4). In cfDNA isolated from plasma before treatment resistance, at a local read depth of 950x, 258 reads (27%) bore the wild-type allele, whereas 711 reads (73%) bore the pathogenic p.R259fs allele (Supplementary Fig. S5). In cfDNA isolated from plasma after treatment resistance, at a local read depth of 968x, 459 reads (44%) bore the wild-type allele. The remaining

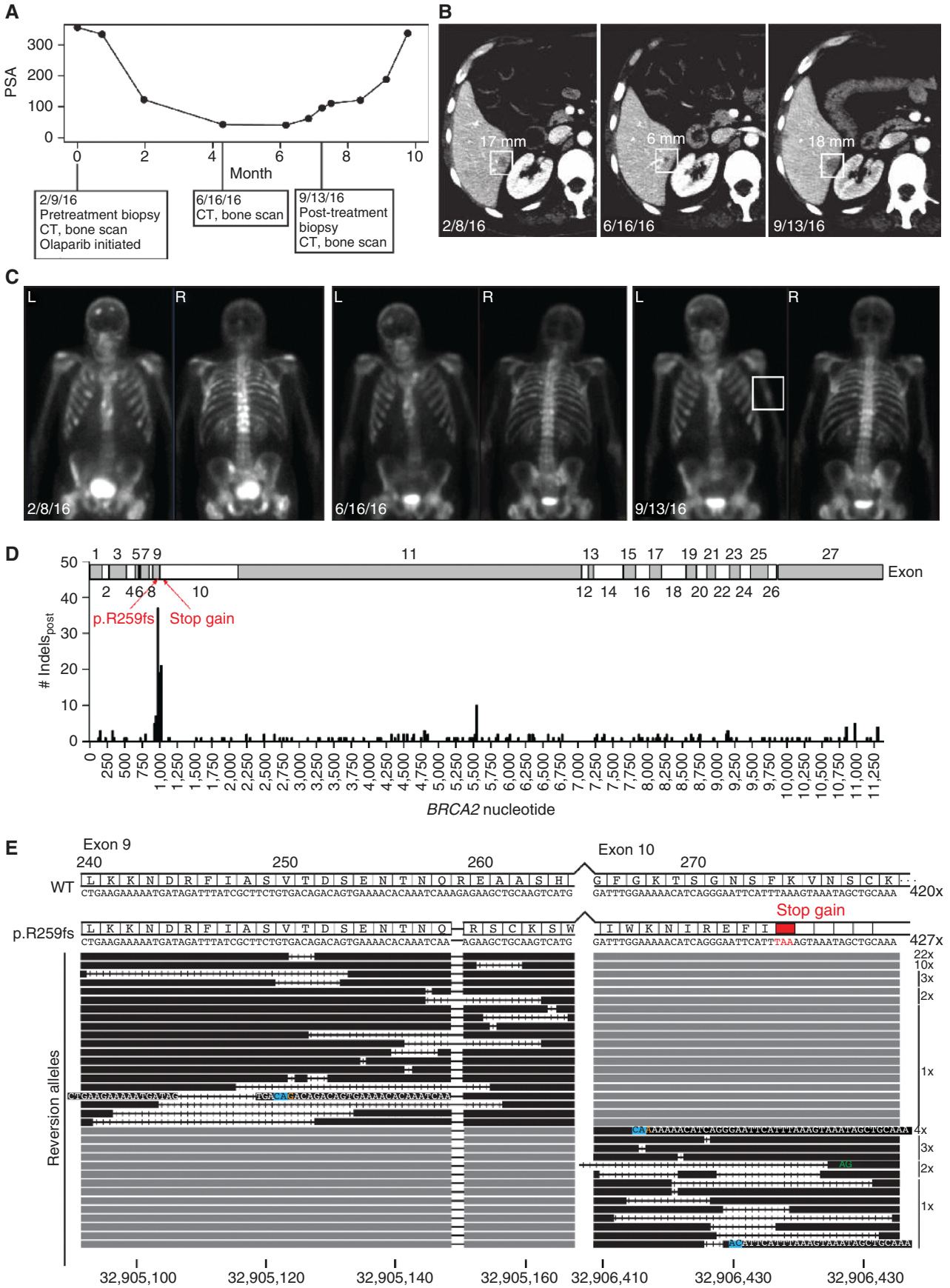

509 reads bore the pathogenic p.R259fs allele. Any combination of somatic insertions or deletions (indels) in the p.R259fs allele that restored the reading frame before the stop-gain at residue 274, and did not produce a new stop-gain, would produce an almost full-length BRCA2 protein. We identified 105 distinct reads bearing somatic alterations beginning upstream of the germline stop-gain mutation, with 82 of these in exons 9 and 10 immediately preceding the stop gain (Fig. 2D). Indel mutations were most frequent immediately upstream of the germline stop-gain mutation, the region *a priori* most likely to harbor reversion mutations. Each of the 34 distinct alleles resulting from indels in this region was predicted to restore the open reading frame of *BRCA2* (Fig. 2E). Predicted protein products from these indels are listed in Supplementary Fig. S6. The number of distinct reads bearing each type of reversion allele ranged from 22 to 1, with deletion sizes ranging from 1 to 42 bp. Reversion indels on exon 9 were confirmed to be in *cis* with p.R259fs, as the tumor bore only one copy of *BRCA2* (Supplementary Fig. S4) and the same DNA read contained both the germline p.R259fs frameshift and the somatic indel.

A total of 82 of the 968 reads in this region (8%) bore an indel. We performed two statistical analyses to support the genetic evidence that indels at this locus, including those observed at low frequency in cfDNA, were likely to represent bona fide reversion alleles. To produce a reversion at this locus, an indel of any size must, when combined with the pathogenic germline deletion of two bp, produce a nucleotide change divisible by three (add 2 bp, lose 1 bp, lose 4 bp, etc.). The probability that 82 randomly generated indels would all be of one of these lengths is $(⅓)^{82}$ or 7.5×10^{-40}. We also compared the length of reversion indels with the length of all 10,652 indels observed in sequenced cfDNA across 73 genes. Indels that produced a predicted reversion were significantly longer than the overall distribution (mean length, 10.2 bp altered; s.d., 12.6 vs. mean length, 1.8 bp altered; s.d., 2.7, $P < 3 \times 10^{-16}$, Wilcoxon rank sum test, Supplementary Fig. S7). This analysis also held for reversion indels supported by a single read (mean length, 15.5; s.d., 15.9, $P = 1.3 \times 10^{-13}$).

DISCUSSION

Here, we report the first mechanistic description of talazoparib resistance, the first *BRCA2* reversion mutations identified in prostate cancer, and the first cases of multiclonal *BRCA2* reversion mutations as a mechanism of PARPi resistance. The multiclonal nature resistance in metastatic disease, in the context of a single evolutionary stimulus, was striking. Based on extrapolation from the ovarian and breast cancer literature, these reversion mutations are likely to confer resistance to platinum-based therapies. The broader impact of this finding for this disease is that it provides a relatively noninvasive readout of resistance to PARP inhibitors, and likely to platinum-based agents, and will allow for personalization of therapy based on this readout. Specifically, in patients with BRCA alterations, the emergence of these reversions at very low PSA levels may allow for switching to non-PARPi and non–platinum-based therapies earlier in the course of disease progression. In addition, for these same patients, significant decreases in cfDNA levels of these reversion mutations on subsequent therapies may signify the emergence of clones that may again be sensitive to PARP inhibition.

These findings highlight the profound selection pressure exerted by PARP inhibitors on BRCA-deficient tumors to restore BRCA function. The 2 patients described in this study were selected for analysis because they responded and then later relapsed on PARPi therapy, and because pre- and post-treatment samples were available. No other patients with *BRCA* mutations were treated with PARPi and had appropriate biopsies or cfDNA samples available for inclusion in this study. Analysis of larger cohorts will provide information about the frequency and kinetics of PARPi reversion mutations in this patient population. Our work further suggests that in order to optimize use of PARPi, strategies will need to be developed to mitigate such mechanisms of resistance. We find that the emergence of somatic genomic alterations conferring treatment resistance can be more comprehensively detected with noninvasive cfDNA approaches capable of capturing genomic alterations from multiple lesions simultaneously. Overall, this study supports the use of cfDNA to identify emergence of reversion mutations conferring resistance to PARPi in the metastatic castration-resistant prostate cancer setting.

METHODS

Exome Sequencing

The studies undertaken were part of an Institutional Review Board–approved protocol. All patients provided written informed consent for the studies performed. Biopsies from bone or liver were fresh-frozen in OCT and preserved in liquid nitrogen. Tissue sections (7 μm) were hematoxylin and eosin (H&E) stained and assessed to be at least 50% tumor. DNA was isolated from five 40 μm tissue sections using the QIAamp Fast DNA Tissue Kit (QIAGEN), with tissue disruption performed by ceramic beads (MP BioMedicals). DNA was quantified by Qubit fluorimeter and verified by a BioAnalyzer DNA 12000 (Agilent). DNA libraries were prepared using 500 ng of DNA as input to the Hyper Kit (Kapa) and barcoded using TruSeq (Illumina), with three cycles of PCR. Whole-exome capture of gene coding regions and

Figure 2. Olaparib resistance in patient 2 was associated with reversion mutations. **A,** Timeline of patient 2's serum PSA level before and during treatment with olaparib, showing a drop in PSA from 355 to a nadir of 40, followed by increase associated with drug resistance. **B,** CT scans from patient 2 pre-olaparib, on treatment, and after resistance show a liver metastasis at 17 mm on February 8, 2016, decreased to 6 mm on June 16, 2016, after olaparib treatment began, and at 18 mm on September 13, 2016, respectively. **C,** Bone scans of patient 2 at times matching **B,** showing widespread metastasis, treatment response, and recurrence of metastatic lesions. **D,** Counts of indels observed exclusively in resistant cfDNA, binned into 50 bp intervals across *BRCA2*. Exon bounds shown at top. The pathogenic stop gain in p.R259fs allele is at nucleotide 1,050, noted with red arrow. **E,** Diagram of *BRCA2* reversion mutation alleles observed in patient 2. Wild-type (WT) *BRCA2* nucleotide and protein sequence, p.R259fs nucleotide and protein sequence, and *BRCA2* reversion alleles present in patient 2's post-olaparib DNA in all of exon 9 and the first 48 nucleotides of exon 10. Black versus gray bars indicate observed versus inferred nucleotide sequence. Deleted nucleotides shown as a thin black line with tics for each deleted nucleotide, insertions highlighted in blue, mutations highlighted in orange, and alternate splice acceptor highlighted in green. For clarity, nucleotides are drawn on reversion alleles where insertions are present; otherwise, nucleotide sequence corresponds to WT. Count of each allele is shown at right.

a small shoulder region of intron–exon boundaries was performed using SeqCap EZ Exome V3 (64.1 Mb; Nimblegen). Library fragment size was verified by BioAnalyzer High Sensitivity DNA Assay (Agilent). Libraries were sequenced on an Illumina HiSeq 4000 instrument. Patient 1's germline, pre-talazoparib, and resistant biopsies were sequenced to a mean depth of 33x, 88x, and 95x, respectively.

FFPE Sequencing

Tumor samples were macrodissected from unstained 5 μm formalin-fixed, paraffin-embedded (FFPE) sections by comparison with an H&E-stained slide. Genomic DNA was extracted using a Macherey-Nagel NucleoSpin Tissue Kit (Clontech). Amplicon libraries were generated from a custom Ion AmpliSeq (Ion Torrent) panel. DNA derived from FFPE (20 ng) was amplified by PCR using AmpliSeq primers and HiFi master mix (Ion AmpliSeq v. 2.0). Amplicons were treated with FuPa (Ion Torrent) to partially digest sequences and phosphorylate amplicons. Library concentration was measured with the Ion Library Quantitation Kit. Libraries were amplified for 20 cycles using emulsion PCR on Ion Sphere particles (ISP) at a 1:2 ratio of library molecules/ISPs (280×10^6 molecules/reaction; Ion Xpress Template Kit version 2.0; Ion Torrent). Positive templated ISPs were biotinylated and enriched with MyOne streptavidin C1 dynabeads (Life Technologies/Thermo Fisher) and sequenced on an Ion Torrent PGM using the Ion PGM 200 Sequencing Kit 2.0, according to the manufacturer's instructions.

cfDNA Sequencing

Whole blood was collected in EDTA, centrifuged at 1,600 rcf, and chilled at 4°C within 2 hours of collection. Plasma and buffy coat were stored at −80°C. Germline DNA was extracted from buffy coat using the DNeasy Blood and Tissue Kit (QIAGEN; manufacturer's instructions) and quantified with a NanoDrop spectrophotometer (Thermo Scientific). Circulating cfDNA was extracted from 6 mL of plasma using the Circulating Nucleic Acids Kit (QIAGEN; manufacturer's instructions) and quantified with a Qubit 2.0 Fluorometer and a Qubit dsDNA HS Assay Kit (Life Technologies). DNA (10 to 100 ng) was used for targeted DNA capture; gDNA was sheared to 180 nt fragments by ultrasonication (Covaris); cfDNA samples do not require shearing. A-tailing, end repair, Illumina-compatible adapter ligation, and between 12 to 17 cycles of PCR amplification were performed. Products were quantified by NanoDrop. Samples were hybridized to a custom NimbleGen SeqCap panel targeting the exonic regions of 73 genes (Supplementary Table S3) for a minimum of 16 hours at 47°C following the SeqCap EZ system protocols. Libraries were purified with AMPure beads (Agencourt) and quantitated by Qubit. Sequencing was performed on an Illumina MiSeq (V3 600 cycle kit). Patient 1's pre-olaparib and resistant cfDNA samples were sequenced to a mean depth of 220x. Patient 2's cfDNA samples were sequenced to a mean depth of 400x (germline) and 1,400x (pre-olaparib and resistant).

Bioinformatics Analysis

FASTQ files from Illumina instruments were aligned against HG19 (genome.ucsc.edu) using BWA version 0.7.12 (16), with duplicates marked using Picard MarkDuplicates version 2.7.1. FASTQ files from Ion Torrent were aligned against HG19 using TMAP version 3.4.1. BAM/SAM file manipulation was performed with SAMtools version 1.3.1 (17). Genotyping was performed using the GATK version 3.3-0-g37228af (18). Functional annotation was performed in ANNOVAR version 2016Feb01 (19). Copy-number calling of solid tumor exomes was performed using CNVkit version 0.8.1 (20). Genome coverage was calculated using bedtools version 2.26 (21). The bounds and frequency of reversion alleles in patient 1's post-talazoparib DNA were defined by DNA reads that included sequence from both sides of the deleted region. Reversion alleles present in patient 1's and patient 2's DNA were identified by visual inspection and Pindel version 0.2.5b9 (Supplementary Methods; ref. 22). Mutation signature analysis was performed in R (23) with the *deconstructSigs* (24) package. Sequencing data are available at synapse.org (doi:10.7303/syn9652227).

PCR Primers and Conditions

PCR amplification was performed on genomic DNA using the primer pair forward: 5′ CTTGATTCTGGTATTGAGCCAGT 3′, reverse: 5′ TGAGCTGGTCTGAATGTTCG 3′, amplified for 35 cycles at an annealing temperature of 62°C with Q5 polymerase (NEB) using the manufacturer's standard conditions. This primer pair was designed to produce a 775 nt product on HG19 reference DNA.

Disclosure of Potential Conflicts of Interest

S. Tomlins is co-founder, consultant, and equity holder at Strata Oncology; reports receiving commercial research support from Astellas, Compendia Biosciences/Life Technologies/ThermoFisher Scientific, and GenomeDX; has received honoraria from the speakers bureaus of AbbVie, Alamac Diagnostics, Astellas/Medivation, Janssen, Roche/Ventana Medical Systems, and Sanofi; has ownership interest (including patents) in Hologic/Gen-Probe Inc.; and is a consultant/advisory board member for AbbVie, Alamac Diagnostics, Astellas/Medivation, Janssen, Roche/Ventana Medical Systems, and Sanofi. A. Ashworth has ownership interest in patents on the use of PARP inhibitors held jointly with AstraZeneca which have benefitted him financially (and may do so in the future) through the ICR Rewards to Inventors Scheme. E.J. Small has received honoraria from the speakers bureau of Janssen and is a consultant/advisory board member for Fortis Therapeutics and Harpoon Therapeutics. F.Y. Feng is a consultant/advisory board member for Clovis, Janssen, and Medivation/Astellas. No potential conflicts of interest were disclosed by the other authors.

Authors' Contributions

Conception and design: D. Quigley, J.J. Alumkal, A. Foye, A. Ashworth, E.J. Small, F.Y. Feng

Development of methodology: A.W. Wyatt, A. Foye, P. Lloyd, J. Youngren, T.M. Beer, F.Y. Feng

Acquisition of data (provided animals, acquired and managed patients, provided facilities, etc.): J.J. Alumkal, A.W. Wyatt, V. Kothari, A. Foye, R. Aggarwal, E. Lu, J. Schwartzman, K. Beja, R. Das, G. Thomas, S. Tomlins, C. Ryan, J. Youngren, T.M. Beer, E.J. Small, F.Y. Feng

Analysis and interpretation of data (e.g., statistical analysis, biostatistics, computational analysis): D. Quigley, J.J. Alumkal, A.W. Wyatt, V. Kothari, P. Lloyd, W. Kim, M. Annala, R. Das, M. Diolaiti, C. Pritchard, G. Thomas, S. Tomlins, K. Knudsen, C. Ryan, T.M. Beer, A. Ashworth, F.Y. Feng

Writing, review, and/or revision of the manuscript: D. Quigley, J.J. Alumkal, R. Aggarwal, W. Kim, M. Diolaiti, C. Pritchard, S. Tomlins, K. Knudsen, C.J. Lord, C. Ryan, J. Youngren, T.M. Beer, A. Ashworth, E.J. Small, F.Y. Feng

Administrative, technical, or material support (i.e., reporting or organizing data, constructing databases): P. Lloyd, E. Lu, J. Schwartzman, J. Youngren, F.Y. Feng

Study supervision: J.J. Alumkal, J. Youngren, A. Ashworth, E.J. Small, F.Y. Feng

Acknowledgments

We thank the men who participated in this study.

Grant Support

This work was supported by a Stand Up To Cancer–Prostate Cancer Foundation–Prostate Dream Team Translational Cancer Research Grant (grant number: SU2C-AACR-DT0812). This research grant is made possible by the generous support of the Movember

Foundation. Stand Up To Cancer is a program of the Entertainment Industry Foundation administered by the American Association for Cancer Research. V. Kothari is supported by a Prostate Cancer Foundation Young Investigator Award. F.Y. Feng and E.J. Small acknowledge support from the Prostate Cancer Foundation. D. Quigley and A. Ashworth acknowledge support from the BRCA Foundation; A. Ashworth acknowledges support from the Breast Cancer Research Foundation and the Susan G Komen Foundation. K. Knudsen acknowledges funding from the Prostate Cancer Foundation.

Received February 8, 2017; revised March 22, 2017; accepted April 26, 2017; published OnlineFirst April 27, 2017.

REFERENCES

1. Breast Cancer Linkage Consortium. Cancer risks in BRCA2 mutation carriers. J Natl Cancer Inst 1999;91:1310–6.
2. Tryggvadottir L, Vidarsdottir L, Thorgeirsson T, Jonasson JG, Olafsdottir EJ, Olafsdottir GH, et al. Prostate cancer progression and survival in BRCA2 mutation carriers. J Natl Cancer Inst 2007;99:929–35.
3. Castro E, Goh C, Olmos D, Saunders E, Leongamornlert D, Tymrakiewicz M, et al. Germline BRCA mutations are associated with higher risk of nodal involvement, distant metastasis, and poor survival outcomes in prostate cancer. J Clin Oncol 2013;31:1748–57.
4. Pritchard CC, Mateo J, Walsh MF, De Sarkar N, Abida W, Beltran H, et al. Inherited DNA-repair gene mutations in men with metastatic prostate cancer. N Engl J Med 2016;375:443–53.
5. Robinson D, Van Allen EM, Wu YM, Schultz N, Lonigro RJ, Mosquera JM, et al. Integrative clinical genomics of advanced prostate cancer. Cell 2015;161:1215–28.
6. Alexandrov LB, Nik-Zainal S, Wedge DC, Aparicio SA, Behjati S, Biankin AV, et al. Signatures of mutational processes in human cancer. Nature 2013;500:415–21.
7. Nik-Zainal S, Davies H, Staaf J, Ramakrishna M, Glodzik D, Zou X, et al. Landscape of somatic mutations in 560 breast cancer whole-genome sequences. Nature 2016;534:47–54.
8. Bryant HE, Schultz N, Thomas HD, Parker KM, Flower D, Lopez E, et al. Specific killing of BRCA2-deficient tumours with inhibitors of poly(ADP-ribose) polymerase. Nature 2005;434:913–7.
9. Farmer H, McCabe N, Lord CJ, Tutt AN, Johnson DA, Richardson TB, et al. Targeting the DNA repair defect in BRCA mutant cells as a therapeutic strategy. Nature 2005;434:917–21.
10. Pommier Y, O'Connor MJ, de Bono J. Laying a trap to kill cancer cells: PARP inhibitors and their mechanisms of action. Sci Transl Med 2016;8:362ps317.
11. Lord CJ, Ashworth A. Mechanisms of resistance to therapies targeting BRCA-mutant cancers. Nat Med 2013;19:1381–8.
12. Edwards SL, Brough R, Lord CJ, Natrajan R, Vatcheva R, Levine DA, et al. Resistance to therapy caused by intragenic deletion in BRCA2. Nature 2008;451:1111–5.
13. Sakai W, Swisher EM, Karlan BY, Agarwal MK, Higgins J, Friedman C, et al. Secondary mutations as a mechanism of cisplatin resistance in BRCA2-mutated cancers. Nature 2008;451:1116–20.
14. Christie E, Fereday S, Doig K, Pattnaik S, Dawson S-J, Bowtell D. Reversion of BRCA1/2 germline mutations detected in circulating tumor DNA from patients with high-grade serous ovarian cancer. J Clin Oncol 2017;35:1274–80.
15. Lord CJ, Ashworth A. BRCAness revisited. Nat Rev Cancer 2016;16:110–20.
16. Li H, Durbin R. Fast and accurate short read alignment with Burrows-Wheeler transform. Bioinformatics 2009;25:1754–60.
17. Li H, Handsaker B, Wysoker A, Fennell T, Ruan J, Homer N, et al. The sequence alignment/map format and SAMtools. Bioinformatics 2009;25:2078–9.
18. McKenna A, Hanna M, Banks E, Sivachenko A, Cibulskis K, Kernytsky A, et al. The Genome Analysis Toolkit: A MapReduce framework for analyzing next-generation DNA sequencing data. Genome Res 2010;20:1297–303.
19. Wang K, Li M, Hakonarson H. ANNOVAR: Functional annotation of genetic variants from high-throughput sequencing data. Nucleic Acids Res 2010;38:e164.
20. U M, Talevich E, Katiyar S, Rasheed K, Kannan N. Prediction and prioritization of rare oncogenic mutations in the cancer Kinome using novel features and multiple classifiers. PLoS Comput Biol 2014;10:e1003545.
21. Quinlan AR, Hall IM. BEDTools: A flexible suite of utilities for comparing genomic features. Bioinformatics 2010;26:841–2.
22. Ye K, Schulz MH, Long Q, Apweiler R, Ning Z. Pindel: a pattern growth approach to detect break points of large deletions and medium sized insertions from paired-end short reads. Bioinformatics 2009;25:2865–71.
23. R Core Team. R: A language and environment for statistical computing. 2012.
24. Rosenthal R, McGranahan N, Herrero J, Taylor BS, Swanton C. DeconstructSigs: delineating mutational processes in single tumors distinguishes DNA repair deficiencies and patterns of carcinoma evolution. Genome Biol 2016;17:31.